ISSN 1590-8844
International Journal of Mechanics and Control, Vol. 17, No. 01, 2016

ENERGY BALANCE AND MECHANICAL BEHAVIOUR OF A FLEXIBLE PNEUMATIC ACTUATOR FOR FISH-LIKE PROPULSION

Andrea Manuello Bertetto* Andrea Cadeddu** Luigi Antonio Besalduch**
Roberto Ricciu** Carlo Ferraresi***

* Department of Mechanical, chemical and material Engineering, University of Cagliari, Italy.

** Department of Civil - Environmental Engineering and Architecture, University of Cagliari, Italy.

*** Department of Mechanical and Aerospace Engineering, Politecnico di Torino, Italy.

ABSTRACT

The paper concerns an evaluation of a flexible actuator performances. The actuator is specially conceived for propulsion of biomorphic fish-like robots. Static and dynamic characteristics are presented, referring to the energy consumption and dynamic performances, evaluated by experimental activity performed by means of a hydraulic channel and by means of specially designed and realised experimental test rigs.

Keywords: Energy balance, bio-mimetic actuator, fish-like robot

1 INTRODUCTION

The robots represent the future in the hard work scenario in the new millennium. More power, precision, stability and repeatability when and where the human work is heavy or the human presence is impossible in hostile environment. The working robots use various types of energy, depending on the mission: electrical power [1], pneumatic [2] etc. for different type of actuators. Pneumatic actuators, in particular, are preferably used for unconventional applications, with customised architectures.
Among the non conventional actuators, the flexible pneumatic actuators are a very interesting proposal; in particular, a significant interest is evoked by the so-called pneumatic artificial muscles [2, 3]. The flexible pneumatic actuators were firstly conceived in 1930 by S. Garasiev, a Russian inventor [4]. One of the most interesting applications of these actuators is in medical field and they have been the input for some industrial and agricultural application. One of the most diffused flexible actuators is the McKibben artificial muscle.

Contact author: A. Manuello Bertetto

Department of Mechanical, chemical and material Engineering, University of Cagliari, Italy.
Via Marengo, 2. 09123 Cagliari, Italy.
Email: andrea.manuello@unica.it

It was designed to be used in an active orthosis for human motion recovery [5]. In any case the flexible actuators are very interesting for applications involving interaction with soft counterparties as in medical applications [6, 7]. The mobility recovery or the blood circulation retrieval by mechanical external actions on the patient [8, 9] are another application of flexible actuators. A very attractive solution for micro grippers for particular tasks as in micro manipulation is represented by flexible pneumatic actuators also in surgical environment.
Flexible pneumatic actuators are also an effective answer to challenging tasks as grasping of delicate objects in agricultural application (i.e. harvesting of agricultural products) or in pipes net inspection or pole climbing [10, 12]. Experimental and theoretical studies, also related to energy consumption, suggested that the flexible actuators may provide effective performances for fish-like propulsion. The classical Gray's studies [13-15], milestone for the research in this field, underlined the interesting advantages of the oscillating tail propulsion. For the tail actuation system, an interesting and innovative choice is represented by the flexible actuators [16-21]. This work is a study of a propulsion for an aquatic fish-like robot, equipped by a particular bending actuator. A specially designed test rig was realised to evaluate the energy consumption performances in the designed fish-like robot, during the operation. In the paper operating characteristic and the energy consumption was referred.

2 EXPERIMENTAL SET-UP AND METHODOLOGY

The actuator has a cylindrical geometry. The actuator body is a rubber made tube with two internal longitudinal chambers divided by a longitudinal wall, in Figure 1 the section of the actuator is presented, as well as the assembled actuator. Around the rubber made cylinder a sequence of aluminium made rings, to prevent radial deformation of the rubber cylinder, are assembled. Two heads, placed at the end of the cylinder, allow the compressed air supply to the two longitudinal chambers and the link to a frame and to the external load. The rubber is an elastomeric material with a 70 shore A hardness; it permits high deformations preserving an elastic behaviour, minimising the residual deformation depending on load velocity. The actuator is a two degrees of freedom device, its workspace is a surface: a two-dimensional plane region. A specially designed experimental set up was realised to trace the workspace of the actuator. This set up is shown in Figure 2.

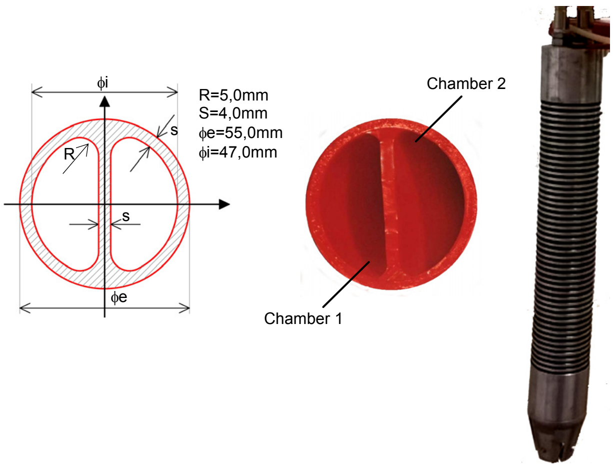

Figure 1 The actuator.

The actuator is vertically suspended to a rigid gantry, shown in Figure 2a, and measuring of the end effector position is performed in a three dimensional space, by means of trigonometric indirect measure. The end effector position, measured at given values of fluid pressures in the chambers, defines the workspace in relation to the chambers' supply pressures. The experimental apparatus, by means of wire position transducers, provides the length variation of the edges of a pyramid having the basis on a horizontal plane and the upper peak linked to the actuator end effector, as represented in Figure 2b. The pneumatic circuit to supply the actuator chambers is schematically drawn in Figure 2c: the two chambers are independently supplied in order to sweep the entire actuator workspace.
The energy consumption of the actuator during its movement was measured by a second test rig, schematically shown in Figure 3.

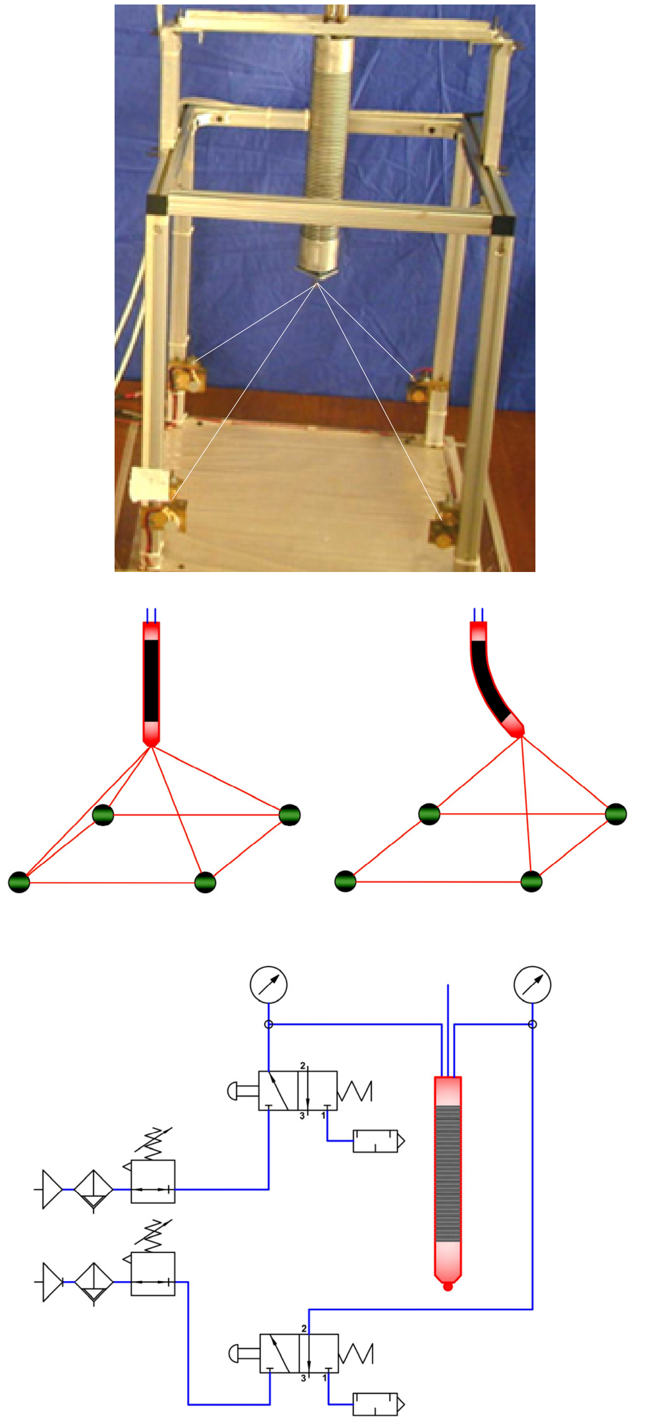

Figure 2 The test rig to trace the actuator workspace.

To control the air volume injected into the actuator a pneumatic cylinder was used (bore diameter 63 mm, stroke 750 mm), whose rod displacement was registered by means of a linear gauge (span 0 ÷ 1270 mm, static sensitivity 9,8455 V/m, repeatability ± 0.02% full stroke), and the pressure by means of two pressure gauges (span 689476 Pa, static sensitivity = 25.0 mV/100kPa).

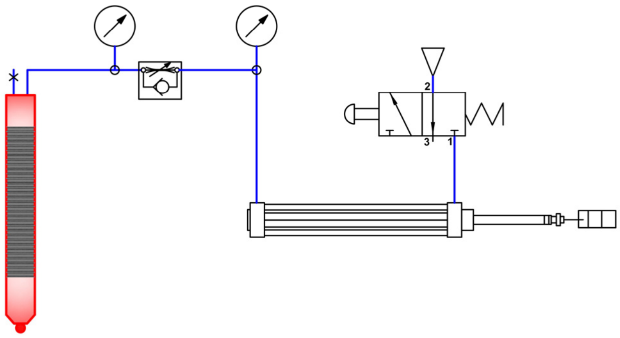

Figure 3 The test rig to evaluate energy consumption by volume and pressure detection.

The position of the flexible actuator was acquired by a digital photo camera. The Data Acquisition System used was: NI USB-6221. The data were acquired and processed by Matlab software.

3 THE WORKSPACE OF THE ACTUATOR

The actuator workspace, represented in Figure 4, is a plane surface perpendicular to the plane of the longitudinal undeformed internal wall dividing the actuator longitudinal chambers. The continuous line has been drawn with a maximum relative pressure of 4 bar. It was traced starting from the end effector (EF) in position A, with both chambers discharged; supplying only chamber 1, EF moves along the A-B curve reaching point B for 4 bar pressure in chamber 1 and ambient pressure in the other one. Maintaining 4 bar pressure in chamber 1 and increasing the pressure in chamber 2 from zero to 4 bar, EF reaches point C, where the fluid pressure is 4 bar in both chambers. By discharging chamber 1, maintaining a pressure of 4 bar relative in chamber 2, the curve C-D is traced. EF reaches again point A when both chambers are discharged. All points inside the edge can be reached by EF, combining the pressures in the chambers within the range 0-4bar relative.

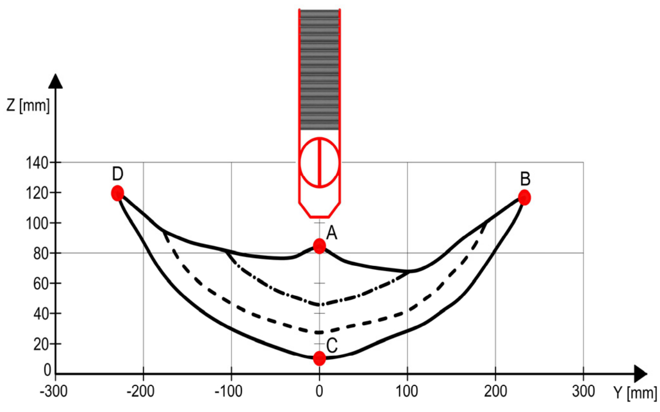

Figure 4 the actuator workspace.

In Figure 4, the bold line represents the workspace limit of the second test rig for a maximum relative pressure of 4 bar. With this set-up only the A-B curve can be drawn, but as it possible to notice, the two lines match quite well, so the behaviour is approximately the same. In Figure 5 the velocity and the acceleration of EF, measured by the second test rig, are shown. It is evident, from the velocity vectors, that the motion trend is very smooth, and also acceleration and deceleration are not so abrupt as in common hydraulic actuator, making this kind of actuator more suitable for the reproduction of fish fin motion.

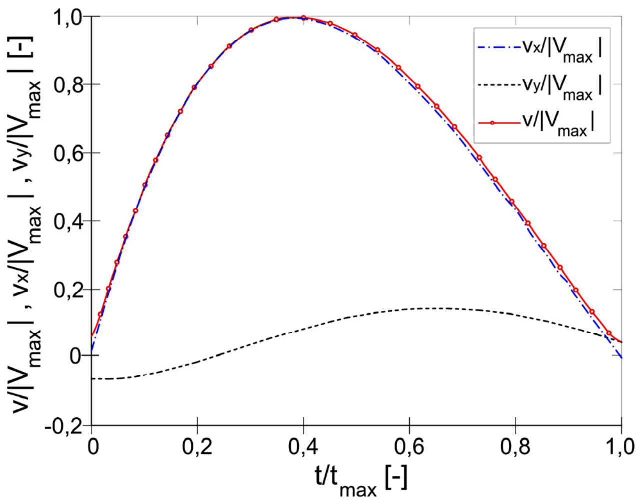

Figure 5 velocity and acceleration of the actuator EF measured by the second test rig.

In particular, the Figure 5 highlights that the velocity is mainly represented by the horizontal component Vx: the longitudinal motion of the EF is not so relevant. In Figure 6 the acceleration components are shown, the acceleration assumes significant values at the edges of the path.

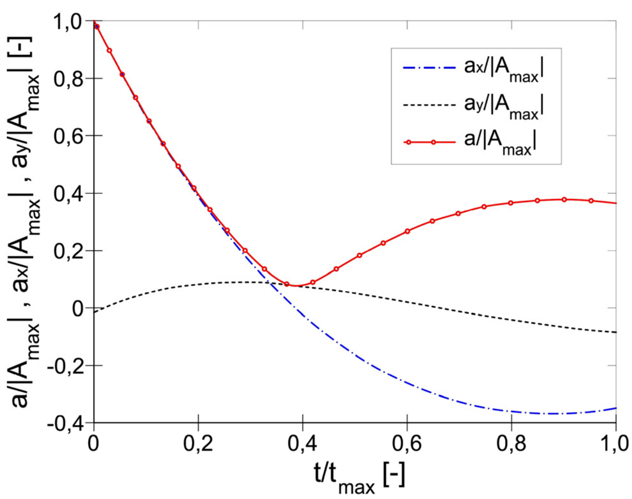

Figure 6 EF velocity components trend vs. time.

These kinematic evaluations can be justified by the Fig. 7, observing the different deformed geometries during the actuator motion. In the Figure 7 (a), without pressure, the actuator is in the rest position. Increasing the relative pressure in one chamber (b), it starts bending, and at approximately 4.5 bar (c) the actuator reaches its maximum curvature. From (a) to (b) the actuator is subjected to an initial stretching phase, whit light curvature, whereupon, from (b) to (c), the stretching stops and the bending behaviour predominate.

4 THERMODYNAMIC CONSIDERATIONS AND ENERGETIC PERFORMANCES

The actuator in the experimental set up (Fig. 3) has been thermodynamically characterized, by the air pressure and volume time recording during the operation.
The task was to know pressure and volume of air inside one actuator chamber during the displacement from initial to final position.
The pressure is measured by two pressure transducers described in the previous paragraph and inserted in the points of the circuit depicted in Figure 3.
The volume is obtained through the indirect measurement of the shift of the piston into the cylinder chamber, whose cross section area is known.
The temperature was measured during the movement of the actuator (sequence a, b, c of Figure 7) and was nearly constant, in the neighbourhood of the room temperature of 20° C.
Therefore the features of the air flow pushed by the piston in the actuator chamber are known.
In the set-up the energy was transferred from the cylinder to the actuator. In particular the energy transfer can be divided in two steps.
At the beginning, both actuator chambers are at atmospheric pressure, see Figure 7a, and the cylinder rod is completely extended.
In the second step the rod performs the complete stroke and the air, firstly in the cylinder posterior chamber, is completely transferred to the actuator that bends as in Figure 7b and finally reaching the configuration as in Figure 7c. The deformed actuator geometries shown in Figure 7 were acquired by digital photo camera.
During the experiment, all main physical quantities, i.e. pressures, volumes and temperatures of the air in cylinder and actuator chambers, were recorded. Figure 9 shows the trend versus the time of the air pressure and volume in the actuator chamber.
The pressure is detected at the inlet port of the actuator chamber and the volume is the indirectly measured by the cylinder rod position, detected by a linear position transducer.

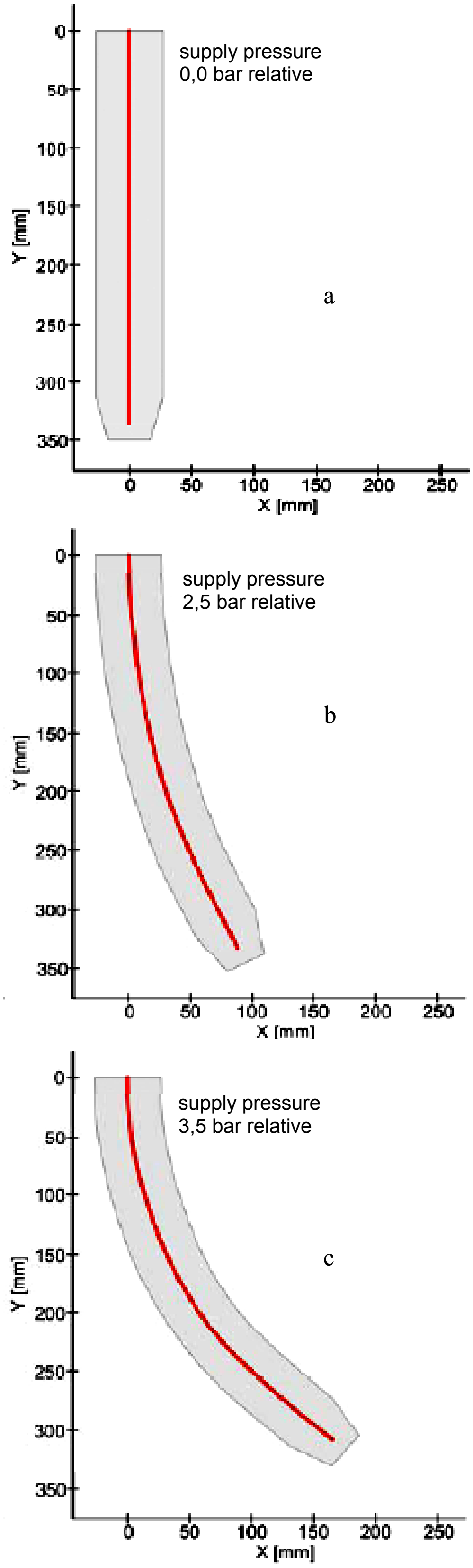

Figure 7 The actuator deformed geometry vs. supply pressure in chamber 1.

The system is considered as an irreversible and closed thermodynamic system. This assumption comes from that there is no temperature variation during the air transfer from cylinder to the actuator chamber: this is because the process is slow and the phenomenon is characterized by lost energy. Moreover no mass transfer exists with respect to the environment. Only heat and mechanical work are considered.
The work in term of infinitesimal variation is:

$$\delta E = P\times\delta V + V\times\delta P \qquad (1)$$

where the work (E) is considered as negative if made by the surrounding. The total work (E) is calculated by integrating the equation (1). This can be done in approximated way considering the whole process as a sequence of small volume variations at constant pressure, therefore the total work was evaluated step by step with the following expression:

$$W = \Sigma Ei = \Sigma(Pi\times\delta Vi) \qquad (2)$$

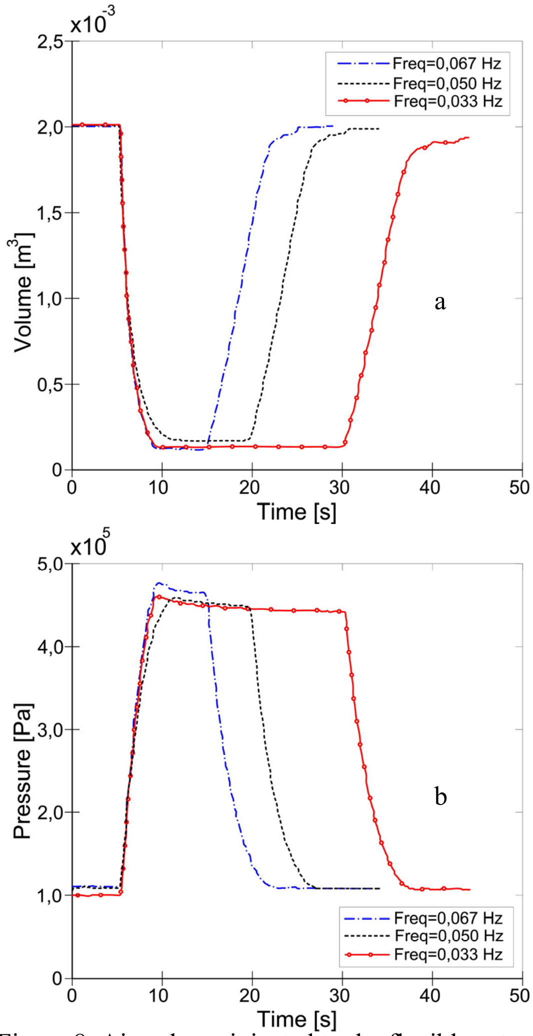

Figure 8 Air volume injected to the flexible actuator (a) and corresponding pressure in the actuator (b) for different oscillating frequencies.

The quantities Pi and δVi, where i = 1,…,N is the number of acquisitions, were measured by the set up described in Figure 2. The curves obtained are represented in Figure 8.
Figures 8a and 8b show the trend of the volume V and of the pressure P vs. time t. Figure 9 shows the phenomenon in the Clapeyron plane (PV), for different frequencies of the compression/expansion cycles. The areas subtended by the curves in the Figure 9 represent the mechanical works: firstly the work is done on the system, subsequently the work is done by the system. The work balance is represented by the net area within the cycle which represents the lost work. The experiment indicates an energy loss of about 47 Joule for each cycle, while the energy retrieved in the return stroke was about 385 Joule. These values are approximately independent from the considered cycle, this suggests that the main losses should be due to the internal friction of the elastomeric actuator material, while the other effects (heat exchange and fluidic resistances) are negligible for slow functioning like in this case. Of course, for higher working frequencies, fluidic losses would have greater influence.

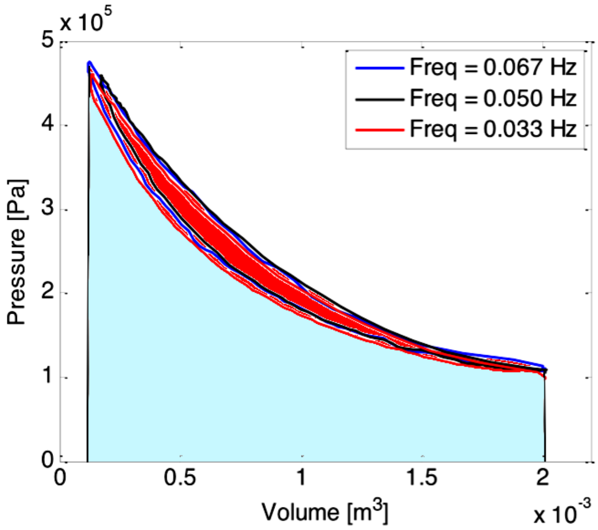

Figure 9 Curves of pressure vs. volume for different oscillating frequencies and in colour area the energy representation.

5 THE ACTUTOR FOR A FISH-LIKE ROBOT PROPULSION

The effectiveness of the actuator for propulsion of a fish-like robot was experimentally verified. The flexible actuator was linked to a tail having geometry referred to that of a carangiform real fish. The flexible actuator was then assembled inside a tapered body, linked to a strain gauges instrumented beam. The robot was then immersed into a hydraulic channel, to measure forces acting on the body in different working conditions.
In Figure 10a the actuator, linked to a carangiform fin, is presented in a bending condition coming from a chamber supply. In Figure 10b the whole robot body is shown.

Figure 10 The actuator and fin integrated system and the fish like robot.

Specific tests were performed in water, using the experimental apparatus schematically shown in Figure 11. Inside the channel, which is 16 m long and 1 m wide, it is possible to generate a water flow rate up to 500 l/s. On the top, a cart can be moved on a rail at a maximum speed of 2 m/s.

The cart is dragged by a wire driven by a controlled electrical motor. The cart carries the measuring system of the strain gauges of the instrumented beam and the PLC aimed at controlling the pneumatic valves to supply the chambers of the flexible actuator. The Figure 11 shows pictures of the channel and the fish-like robot suspended to an instrumented beam to detect the forces acting on the robot along the channel axis. During the actuator motion, for a given water velocity, the net force acting on the robot was measured. A drawing of the robot linked to the instrumented beam shows the device encumbrances. The robot body is 1100mm overall long and the transversal fin dimension is 360mm, the body has a diameter of 180mm.
In a separate test the resistance of the robot, for different fluid velocities and motionless actuator, was measured. The fin-actuator thrust is taken as the sum of resistance and net force. In the photographs of Figure 12 the channel and the experimental equipment are shown. The most relevant details are the channel transparent lateral side, the water free surface, the rail on the channel and the instrumented bar to detect the force acting on the immersed fish like robot.

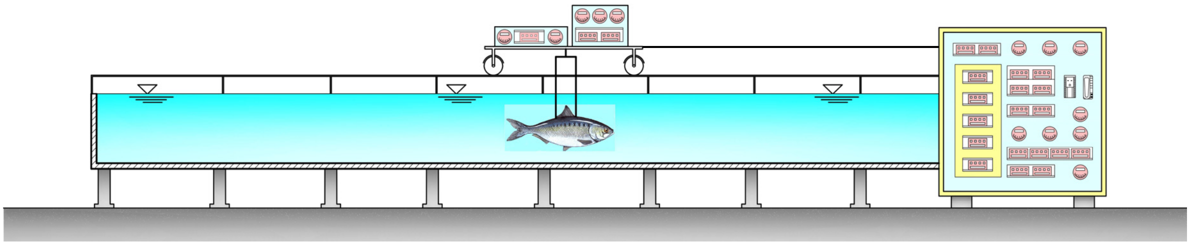

Figure 11 The hydraulic channel scheme.

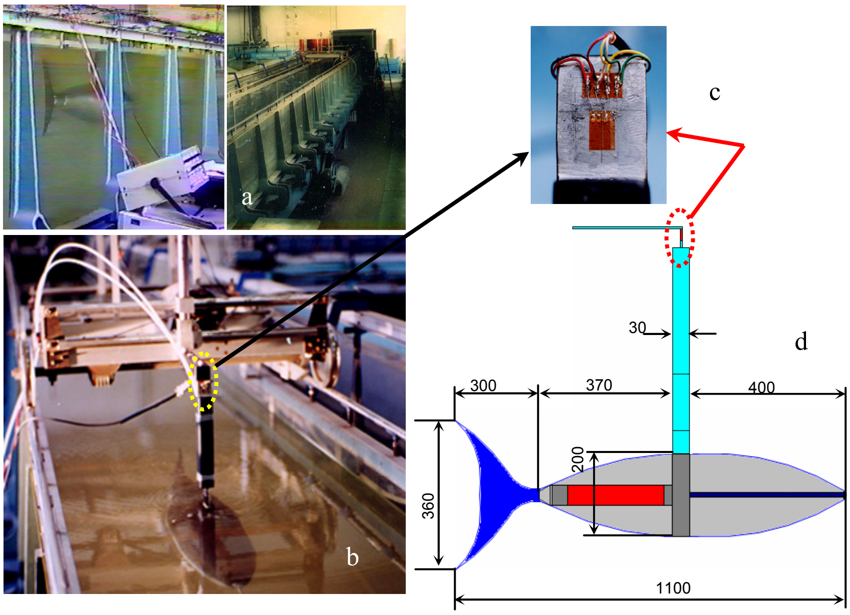

Figure 12 The hydraulic channel. It is possible to see the channel transparent lateral side (a), the water free surface and the immersed fish like robot, as the rail on the channel (b) and the instrumented bar to detect the force acting on the immersed fish like robot schematically represented in (d).

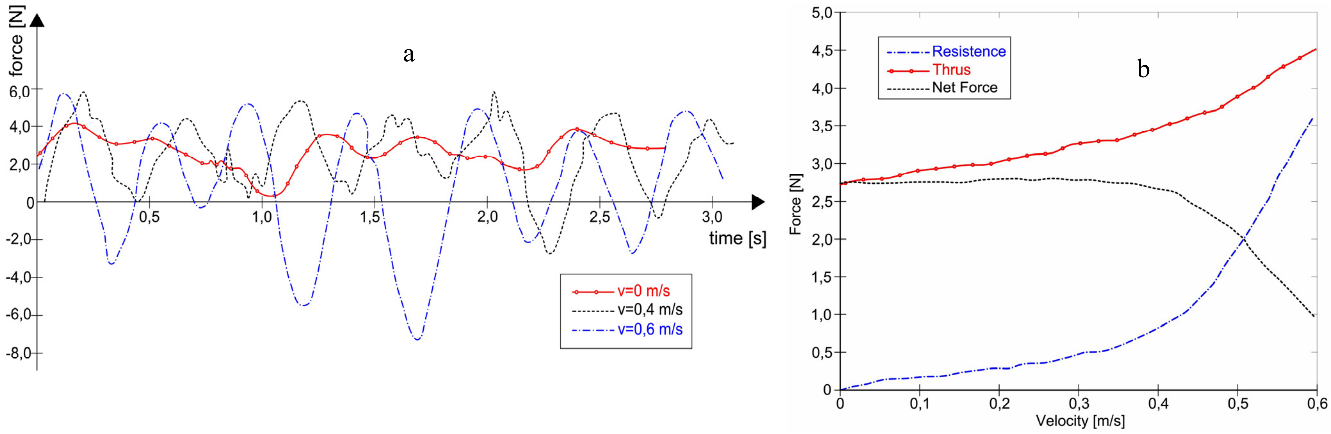

Figure 13 Force acting on the fish-like robot in the channel. (a): total measured force vs. time, at different water velocities; (b): mean values of resistance, thrust and net forces versus robot velocity in water.

The oscillating tail frequency, during in-channel tests, was 0.5 Hz, and a pneumatic supply pressure of 5 bar relative was given to perform an arc amplitude of the tail oscillating motion of 0.5m of the centre of the tail. The graphs of Figure 13a, at the left side, show the values of forces vs. time, during the oscillatory motion of the fin for three different water velocity values: 0, 0.4 and 0.6 m/s. The graphs of Figure 13b, at the right side, show the average force values in a fin oscillating period vs. robot velocity in water. The tree curves reported in Figure 13b represent: (i) the net force, obtained as a mean in time of the measured force values, dragging the robot at given velocity respect to the water; (ii) the resistance, measured directly dragging the fish, at different velocities, with non operating tail; (iii) the thrust of the tail, computed as the sum of the previously described force components. As it can be seen, the net force, acting on the immersed robot, is positive up to a robot velocity of about 0.6m/s relative to water.

6 CONCLUSIONS

This work investigated the performances of a flexible bending pneumatic actuator, designed for aquatic propulsion driving the oscillating motion of a fish-like fin. The experimental tests confirmed effective performances of the actuator as regards the propulsion capability, on the other hand, the experiment highlighted the performances from an energetic point of view. The study allowed to individuate the main problems that have to be faced and solved in future work, namely optimization of the fluid power transmission and the choice of materials with low internal friction for the actuator’s body.

AKNOWLEDGEMENTS

This research was founded by the Italian Ministry of Research (MIUR).

REFERENCES

[1] Chaari M.Z., Applied to charge wirelessly the batteries of gas and petroleum pipes crawlers. *PowerWave: - 8th International Workshop of NDT Experts, Proceedings*, pp. 65-68, 2015.

[2] Ferraresi C., Franco W., Manuello Bertetto A., Flexible Pneumatic Actuators: a comparison between the McKibben and the straight fibres muscle. *J. of Robotics and Mechatronics*, 13-1, pp. 56-63, 2001.

[3] Ball E., Lin Y., Garcia E., Characterization and modeling of geometric variations in McKibben pneumatic artificial muscles, *Proceedings of SPIE - The International Society for Optical Engineering*; 8686, 868605, 2013.

[4] Palko A., Smrček J., The use of pneumatic artificial muscles in robot construction, *Industrial Robot: An International Journal*, Vol. 38 Iss: 1, pp.11–19, 2011.

[5] Schulte H. F., The characteristics of the McKibben artificial muscle. The Application of External Power in Prosthetics and Orthotics, Appendix H, , Publ. 874, *National Academy of Sciences, Washington, D.C.*, pp. 94-115, 1961.

[6] Watanabe Y., Maeda M., Yaji N., Nakamura R., Iseki H., Yamato M., et al., Small, soft, and safe microactuator for retinal pigment epithelium transplantation, *20th IEEE International Conference on Micro Electro Mechanical Systems (MEMS 2007)*, Kobe, Japan, pp. 494–497, 2007.

[7] Shimizu K., Mori Y., Hayashi K., Shunori A., Kawakami S., Hashida M., et al., Genedelivery in mice using an implanted pneumatically actuated microsystem. *Micro Electro Mechanical Systems (MEMS), in: 24th International Conferenceon IEEE*, pp. 181–184, 2011.

[8] Manuello Bertetto A., Meili S., Concu A., Crisafulli A. An Inflatable Pneumatic System For Blood Pressure Recovery, Mechanics Based Design of Structures and Machines, *Taylor and Francis* 40-4, pp. 506-518, 2012.

[9] Manuello Bertetto A., Meletti M., Mechatronic Device for Stimulating the Blood Circulation: Design and Implementation, *RAAD 2013 – 22nd International Workshop on Robotics in Alpe Adria Danube Region*, September, Portorose, Slovenia 11-13, 2013.

[10] Yu, L.Z.: Study on a pneumatic inspection micro robot, *Applied Mechanics and Materials* 519-520, pp. 1327-1330, 2014.

[11] Manuello Bertetto A., Ruggiu M., Pneumatic Robot for Pipe Inspection, International Journal of Mechanics and Control, Vol. 2 No. 2, 2001.

[12] Manuello Bertetto A., M. Ruggiu M., Pole Climbing Pneumatic Robot, Proceedings of the Fifth JFPS International Symposium on Fluid Power, pp. 43-48, 2002.

[13] Gray J., Studies in animal locomotion I. The movement of fish with special reference to the eel., *J. Exp. Biology*, 10, pp. 88-104, 1933.

[14] Gray J., Studies in animal locomotion II. The relationship between the waves of muscular contraction and the propulsive mechanism of the eel. *J. Exp. Biology*, 10, pp. 386-390, 1933.

[15] Gray J., Studies in animal locomotion III. The propulsive mechanism of whiting. *J. Exp. Biology*, 10, pp. 391-400, 1933.

[16] Shao J., Wang L., Yu J., Development of an artificial fish-like robot and its application in cooperative transportation, *Control Engineering Practice*. 16, pp 569–584, 2008.

[17] Cataudella C., Ferraresi C., Manuello Bertetto A., Flexible actuator for oscillating tail marine robot, Int. *Journal of Mechanics and Control*, Torino, 2, pp.13-21, 2001.

[18] Manuello Bertetto A., Ruggiu M.: Tail Actuator Propulsion Device for Aquatic Robot, *J. of Robotics and Mechatronics*, 18-1, pp. 80-90, 2006.

[19] Manuello Bertetto A. Underwater robots: a fascinating challenge. Chapter 4. *Mobile Robots for Dynamic Environments*, ed. Faruk Kececi and Marco Ceccarelli. New York, NY: ASME Press, pp. 1-21, 2015.

[20] Clark A.J., Tan X., McKinley P.K., Evolutionary multiobjective design of a flexible caudal fin for robotic fish, *Bioinspiration and Biomimetics* Volume 10, Issue 6, Article number 065006, doi:10.1088/1748-3190/10/6/065006, 2015.

[21] Bertetto A.M., Ferraresi C., Besalduch L.A., Ricciu R., Cadeddu A., Flexible actuator for biomorphic applications: Performances and energy consumption evaluation, *Advances in Intelligent Systems and Computing* Volume 371, pp. 115-123, 2016.